

A New Flexible Approach to Estimate Highly Nonstationary Signals of Long Time Duration

Meryem Jabloun, François Léonard, Michelle Vieira, Nadine Martin

▶ **To cite this version:**

Meryem Jabloun, François Léonard, Michelle Vieira, Nadine Martin. A New Flexible Approach to Estimate Highly Nonstationary Signals of Long Time Duration. IEEE Transactions on Signal Processing, 2007, 55 (7), pp.3633-3644. hal-00112552

HAL Id: hal-00112552
https://hal.science/hal-00112552

Submitted on 20 Dec 2007

HAL is a multi-disciplinary open access archive for the deposit and dissemination of scientific research documents, whether they are published or not. The documents may come from teaching and research institutions in France or abroad, or from public or private research centers.

L'archive ouverte pluridisciplinaire **HAL**, est destinée au dépôt et à la diffusion de documents scientifiques de niveau recherche, publiés ou non, émanant des établissements d'enseignement et de recherche français ou étrangers, des laboratoires publics ou privés.

A New Flexible Approach to Estimate the IA and IF of Nonstationary Signals of Long-Time Duration

Meryem Jabloun, Francois Leonard, Michelle Vieira, and Nadine Martin, *Member, IEEE*

***Abstract*—In this paper, we propose an original strategy for estimating and reconstructing monocomponent signals having a high nonstationarity and long-time duration. We locally apply to short-time duration intervals the strategy developed in our previous work about nonstationary short-time signals. This paper describes a nonsequential time segmentation that provides segments whose lengths are suitable for modeling both the instantaneous amplitude and frequency locally with low-order polynomials. Parameter estimation is done independently for each segment by maximizing the likelihood function by means of the simulated annealing technique. The signal is then reconstructed by merging the estimated segments. The strategy proposed is sufficiently flexible for estimating a large variety of nonstationarity and specifically applicable to high-order polynomial phase signals. The estimation of a high-order model is not necessary. The error propagation phenomenon occurring with the known approach, the higher ambiguity function (HAF)-based method, is avoided. The proposed strategy is evaluated using Monte Carlo noise simulations and compared with the Cramér–Rao bounds (CRBs). The signal of a songbird is used as a real example of its applicability.**

***Index Terms*—Cramér–Rao bounds (CRBs), maximum likelihood, nonlinear modulation, nonstationary signal, polynomial phase signal, simulated annealing, time frequency (TF).**

I. Introduction

THIS paper is concerned with the commonly encountered problem of estimating signals that show nonlinear amplitude and frequency (AM/FM) modulations and are embedded in an additive noise. These nonstationary signals are widely used in various applications including radar, sonar, mechanics, speech, biomedicine, and communications [1]–[5].

The observed noisy signal $y[n]$ is defined as follows:

$$y[n] = s[n] + e[n], \qquad \text{for} \quad 0 \le n \le N-1 \tag{1}$$

$$s[n] = A[n]e^{j\Phi[n]} \tag{2}$$

where $s[n]$ represents the noise-free signal and $e[n]$ a white complex Gaussian noise with zero mean and unknown variance σ^2. N is the total sample number and j is the complex number verifying $j^2 = -1$. $A[n]$ and $\Phi[n]$ are the instantaneous amplitude (IA) and phase, respectively. The instantaneous frequency (IF) is defined by a numerical derivation of $\Phi[n]$

$$F[n] = \frac{1}{2\pi}\left(\Phi[n+1] - \Phi[n]\right). \tag{3}$$

The IA and IF are both time-varying functions and IF verifies $0 < F[n] < (F_s/2)$ in relation to Shannon's theorem, F_s being the sampling frequency. To remove the ambiguity in the definition of the amplitude and phase of the signal model (2), we assume $\Phi[n]$ is nondiscontinuous and $A[n]$ is real and positive [6].

A. Overview of Existent Techniques

The estimation of nonstationary signals, in particular, polynomial phase signals (PPS), received considerable attention and many techniques have already been proposed [7]–[16]. We present some of the current techniques based on polynomial modeling. The IA and phase are approximated by

$$\begin{aligned} A[n] &= \sum\nolimits_{m=0}^{P} \alpha_m n^m, \\ \Phi[n] &= \sum\nolimits_{m=0}^{Q} \beta_m n^m, \end{aligned} \qquad \text{for} \quad 0 \le n \le N-1 \tag{4}$$

where α_m and β_m are the real coefficients of the decomposition of $A[n]$ and $\Phi[n]$, respectively. P and Q are approximation orders of $A[n]$ and $\Phi[n]$, respectively, and need to be estimated in many application fields.

In [7], the higher ambiguity function (HAF), which is a suboptimal method compared with the maximum-likelihood procedure, was used to estimate PPS. The HAF technique involves transforming the Qth-order PPS given by (4) into a single harmonic at a frequency proportional to the Qth-order coefficient β_Q (4). The basic idea comes from the fact that $(\Phi[n]-\Phi[n-\tau])$ is a $(Q-1)$th-order polynomial, τ being a constant lag. When the estimation $\hat{\beta}_Q$ is computed, the algorithm is repeated for $y[n]$ multiplied by $e^{-j\hat{\beta}_Q n^Q}$ which becomes a $(Q-1)$th PPS. This compensation induces error propagation from the highest order coefficient to the lowest one and it drastically reduces the HAF estimation performance. Moreover, a compromise is necessarily made between the order determination of the PPS model and available signal-to-noise ratios (SNRs). Many techniques based on the HAF are proposed to improve the estimation [15], [17]–[19].

In [10] and [20], a Bayesian approach for estimating monocomponent PPS was proposed. In [10], the amplitude was considered constant and a simultaneous estimation of the polynomial phase parameters and the approximation order Q was achieved. A reversible jump Monte Carlo Markov chain method based on a Metropolis–Hastings algorithm is employed to sample from the marginal posterior distribution of the model

Manuscript received May 17, 2006; revised November 8, 2006. The associate editor coordinating the review of this manuscript and approving it for publication was Dr. Antonio Napolitano.

M. Jabloun, M. Vieira, and N. Martin are with the GIPSA-Lab/INPG-CNRS, Laboratoire des Images et des Signaux, 38402 Saint Martin d'Heres, France (e-mail: meryem.jabloun@lis.inpg.fr; nadine.martin@lis.inpg.fr; michelle.vieira@lis.inpg.fr).

F. Leonard is with the Institut de recherche d'Hydro-Quebec, 1800 Varennes, QC, Canada (e-mail: leonard.francois@ireq.ca).

Color versions of one or more of the figures in this paper are available online at http://ieeexplore.ieee.org.

Digital Object Identifier 10.1109/TSP.2007.894254

1053-587X/$25.00 © 2007 IEEE

parameters. This technique is efficient to estimate linear or quadratic FM signals; however, the estimators become very biased when a higher order PPS with a time-varying amplitude is considered.

On the other hand, other techniques which were recently published do not suppose polynomial modeling [21], [22]. In [22], the tracking of the frequency and amplitude evolution is performed from the spectrogram and particle filtering. This supposes a frequency/amplitude evolution model with respect to time $A_n = A[n]$ and $F_n = F[n]$. The unknown parameters A_n and F_n and the component number K_n are estimated online. The method is applied to multicomponent signal with linear FM, the amplitude being constant. This method enables the estimation of the signal component number and the detection of their birth and death at high SNRs. However, adapting this algorithm for processing highly nonlinear AM/FM signals needs to determine the adequate proposal density.

B. Contribution of the Paper

We propose a new flexible approach for fitting a wide variety of signals with highly nonlinear AM/FM defined as in (2). It is based on a recent analysis of signals having short-time duration and nonlinear AM/FM [23]–[25]. In those papers, the IA and IF are both approximated by low-order polynomials. A discrete orthonormal polynomial base is derived and contributes in the performance enhancement. The model parameters are estimated using a maximum-likelihood procedure known to possess optimality property. As this leads to a multivariate nonlinear equation to be minimized, a stochastic optimization technique based on the simulated annealing method is used. The variances of the mean-square-estimation errors (MSEs) of the model parameters are close to the derived Cramér–Rao bounds (CRBs) (which are functions of the SNRs). Results obtained through the proposed method show better accuracy at low SNRs (0 dB) when compared to those obtained by using the HAF-based method. Motivated by the efficiency and the optimality of this method, the estimation of highly nonlinear AM/FM signals of long-time duration is addressed in this paper.

Unlike (4), which considered polynomial models requiring a large number of parameters, we use a local approach. The main contribution of this paper is a strategy for extracting short-time segments from a long-time signal. This extraction is not ordered through time; the length, the position, and the number of segments are estimated using any nonnegative time-frequency distribution (TFD) without cross terms. In the proposed algorithm, we start by finding short-time segments whose lengths are suitable for approximating locally both the IA and IF by low-order polynomial models. The lengths vary from one segment to another and segments can overlap.

Fig. 1 illustrates the principle with a signal whose IA and IF are third- and seventh-order polynomials, respectively. Examples of the short-time segments considered are shown in Fig. 1 as adapted to a second-order polynomial approximation; $(S1)$, $(S2)$, and $(S3)$ are three segments of 55, 63, and 51 samples, respectively. The estimation of the local-model parameters is subsequently achieved for each segment using the procedure developed in [23]–[25]. The estimation and reconstruction of the entire signal is accomplished by the merging of all the estimated

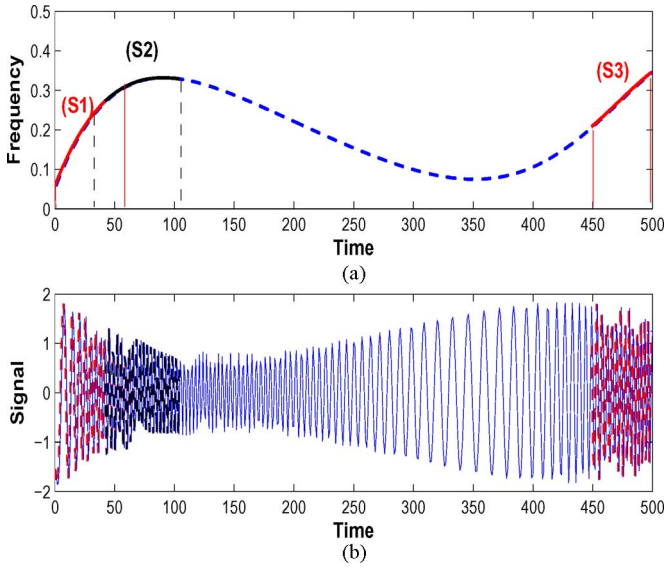


Fig. 1. Examples of short-time segments adapted to a second-order polynomial modeling: (a) IF and (b) the signal. (S1), (S2), and (S3) are three segments of 55, 63, and 51 samples, respectively. The IA and IF are third- and seventh-order polynomials, respectively.

segments. We emphasize the flexibility and the potential of the strategy proposed for dealing with a wide range of nonlinear AM/FM signals. Only low-order models with a low number of parameters are used and the effect is a significant improvement of the estimation accuracy.

This paper is structured as follows. In Section II, the short-time duration model proposed in [23]–[25] is recalled. The time-segmentation strategy and the merging process are detailed in Section III. The performance of the proposed approach and a comparison to the HAF-based method are presented in Section IV. An application to a real signal is also given in Section V. Finally, Section VI summarizes our work and describes the direction that future work could take.

II. Local AM/FM Model

Let us consider short-duration intervals (segments) where low-order polynomial functions are appropriate for approximating uniformly both IF and IA according to Weierstrass' theorem. Examples of such intervals are shown in Fig. 1. We proceed as described in [24] for the parameter estimation.

A. Local AM/FM Polynomial Modeling

On each segment, the local IA $a[k]$, IF $f[k]$, and instantaneous phase $\varphi[k]$ are defined by

$$\begin{aligned} a[k] &= A[n_0+k], \\ f[k] &= F[n_0+k], \\ \varphi[k] &= \Phi[n_0+k], \end{aligned} \qquad \text{for} \quad \frac{-L}{2} \le k \le \frac{L}{2} \tag{5}$$

where n_0 indicates the segment center, $k = n - n_0$ is the time referenced to the segment center, and $L+1$ is the segment length assumed to be odd in order to simplify the algorithm implementation. $a[k]$ and $f[k]$ verify the same constraints as $A[n]$ and $F[n]$

$$0 < a[k] \quad \text{and} \quad 0 < f[k] < \frac{F_s}{2}. \tag{6}$$

The local polynomial model is then defined by

$$\begin{aligned} a[k] &= \sum_{m=0}^{p} a_m g_m[k] \\ f[k] &= \sum_{m=0}^{q} f_m g_m[k] \\ \varphi[k] &= \varphi_0 + 2\pi \left(\sum_{l=-\frac{L}{2}}^{k} f[l] - \sum_{l=-\frac{L}{2}}^{0} f[l] \right) \end{aligned} \tag{7}$$

where p and q are the polynomial approximation orders of $a[k]$ and $f[k]$, respectively, and $g_m[k]$ is a discrete polynomial of order m. The real coefficients of the decomposition of $a[k]$ and $f[k]$ on the discrete polynomial base $(g_m[k])_{m=0,\ldots,\max(p,q)}$ are a_m and f_m, respectively. In order to reduce the estimation error [26], $\varphi[k]$ is referenced to the segment center; we have $\varphi[0] = \Phi[n_0] = \varphi_0$ where φ_0 is the original phase related to the considered segment. Therefore, we have to estimate for each local model a vector of $p+q+3$ parameters

$$\boldsymbol{\theta} = [a_0, a_1, \ldots, a_p, \varphi_0, f_0, f_1, \ldots, f_q]^{\mathrm{T}}. \tag{8}$$

To reduce the number of parameters to be estimated for each segment, the polynomial approximation orders p and q are limited. The segment length $L+1$ is selected in Section III-A such as p and q satisfying

$$0 \leq \min(p,q) \leq \max(p,q) \leq 3. \tag{9}$$

In [24], we calculated an orthonormal discrete polynomial base $g_m^D[k]$ by applying the Gram–Schmidt procedure. The first three polynomials are reproduced in Section A of the Appendix. The comparison with other polynomial bases shows that the orthonormality property enhances the estimation efficiency by significantly reducing the parameter coupling. Recently, we found the base $g_m^D[k]$ is linearly related to the discrete Legendre polynomial one $g_m^{DL}[k]$ [27]

$$g_m^D[k] = (-1)^m g_m^{LD}\left[k + \frac{L}{2}\right]. \tag{10}$$

$g_m^{LD}[k]$ is given for $0 \leq i \leq L+1$ by

$$g_m^{LD}[i] = \frac{1}{C_m^L} \sum_{u=0}^{m} (-1)^u \binom{u}{m} \binom{u}{m+u} \frac{i^{\{u\}}}{(L+1)^{\{u\}}} \tag{11}$$

where $i^{\{u\}} = i(i-1)\ldots(i-u+1)$ is the backward factorial function of order u, $(C_m^L)^2 = ((L+2+m)^{\{m+1\}}/(2m+1)(L+1)^{\{m\}})$ is the square of the scaling normalization coefficient, and $\binom{m}{u} = m!/(u!(m-u)!)$ is the binomial coefficient.

B. Maximum-Likelihood Estimation

To benefit from the optimality, a maximum-likelihood procedure is locally used for parameter estimation. This is equivalent to minimization of the least-square (LS) function for Gaussian noises and thus results in the following nonlinear equation:

$$\widehat{\boldsymbol{\theta}} = \underset{\boldsymbol{\theta} \in \mathbb{R}^{p+q+3}}{\arg\min}\ \ell_{\mathrm{LS}}(\boldsymbol{\theta}), \tag{12}$$

with

$$\ell_{\mathrm{LS}}(\boldsymbol{\theta}) = \sum_{k=\frac{-L}{2}}^{\frac{L}{2}} |y_l[k] - s_l[k]|^2. \tag{13}$$

$y_l[k]$ and $s_l[k]$ are the local noisy signal and the local noise-free signal, respectively

$$\begin{aligned} y_l[k] &= y[n_0+k], \\ s_l[k] &= s[n_0+k] = a[k]e^{j\varphi[k]}, \end{aligned} \qquad \text{for} \quad \frac{-L}{2} \leq k \leq \frac{L}{2}. \tag{14}$$

The LS function $\ell_{\mathrm{LS}}(\boldsymbol{\theta})$ (13) is multidimensional and nonlinear with respect to $\boldsymbol{\theta}$ (8). The estimation of $\boldsymbol{\theta}$ by direct minimization is extremely difficult and classical optimization techniques such as gradient descent, Gauss–Newton, and expectation–maximization (EM) algorithm do not ensure convergence to the global minimum in the presence of many local extrema. To overcome this problem, there is a variety of meta-heuristic approaches for escaping local extrema. We use the simulated annealing, which Monte Carlo simulations in [23] and [24] have shown perform well in terms of low bias and small MSEs. The main steps of the simulated-annealing-based algorithm are detailed in Section B of the Appendix.

III. Time-Segmentation strategy

This section details the strategy used to obtain short-duration segments adapted to a low-order polynomial approximation for both the local IA and IF. The merging process of all local models is also described.

First, a rough approximation of $F[n]$ denoted by $F_0[n]$ is determined using any nonnegative TFD without cross terms [28]. Let us denote by $S_y[n,\nu]$ the TFD of the noisy signal $y[n]$ defined in the time (n) and frequency (ν) domain. Since $y[n]$ is a single component, the time-frequency (TF) plan is composed of one ridge of energy. This ridge creates a TF trajectory, which we consider as the IF approximation $F_0[n]$

$$\forall n = 0, \ldots, N-1 \qquad F_0[n] = \underset{\nu}{\arg\max} |S_y[n,\nu]| \tag{15}$$

where $|.|$ is the modulus. There are then two main steps to perform the whole signal estimation.

A. Segment Extraction

To extract the first segment to be processed, the point of the signal with the highest energy content is located in the TF plan by finding the peak coordinates n_0 and ν_0 of the TFD energy

$$[n_0, \nu_0] = \underset{n,\nu}{\arg\max} |S_y[n,\nu]|. \tag{16}$$

Then, the time interval $[n_0 - (L/2), n_0 + (L/2)]$ is centered on this energy peak and the segment length $L+1$ is selected in such a way that a simple LS fitting of $F_0[n]$ on $[n_0-(L/2), n_0+(L/2)]$, with a low-order polynomial (9), is possible with a reasonable LS error. This step is detailed in Table I. Then, the estimation of the local frequency $f[k]$ and amplitude $a[k]$ is carried out as described in Section II using (7) and (12)–(14). The local decomposition of $F_0[n]$ on the chosen polynomial base provides

TABLE I
SEGMENT DEFINITION

- Set $L = \mathsf{E}[\nu_0^{-1}]$, $\mathsf{E}[.]$ being the nearest even number. ν_0 is given by (16).
- Select a set of successively increasing window lengths $L \leq L_1 \leq L_2 \leq \ldots \leq L_{Max}$, where $L_{i+1} = L_i + 2$. Let $S_1, S_2, \ldots, S_{Max}$ be the segments centered around n_0, whose lengths are $L_1, L_2, \ldots, L_{Max}$ respectively.

1. Start with $i = 1$ and $q = 0$.
2. Fit $F_0[n]$ on S_i, with a polynomial $\mathcal{P}_{q,i}[n]$ of order q, by simple LS fitting. Evaluate LS error $e_{LS}(S_i) = \sum_{n \in S_i} |\mathcal{P}_{q,i}[n] - F_0[n]|^2$.
3. If $e_{LS}(S_i) \leq \epsilon$ increase $i = i + 1$. Otherwise increase $q = q + 1$. Stop if $q > 3$ or $L_i > L_{Max}$.
4. S_{i-1} and $q = q-1$ are the segment and the frequency approximation-order outputs respectively.

Remark: *By experiment, we recommend using* $L_1 \geq 15$, $L_{Max} \leq 61$ *and* $\epsilon \approx 0.1$ *for most investigated signals.*

a good initialization of the model parameters (see Section B of the Appendix). To find the next segment, we remove $\hat{s}_l[k]$ the estimate of $s_l[k]$ (14) from the noisy signal $y[n]$

$$\begin{aligned} y_r[n] &= y[n] - \hat{s}_l[n - n_0], \quad \text{for } n = n_0 - \tfrac{L}{2}, \ldots, n_0 + \tfrac{L}{2} \\ &= y[n], \qquad\qquad\qquad\quad \text{else.} \end{aligned} \tag{17}$$

We compute $S_{y_r}[n, \nu]$ the TFD of the residue $y_r[n]$, which provides the next energy peak (16). Then, the length of a new segment is determined in the same way as the first one (Table I). The time position and length of a new segment are dependent from the residue $y_r[n]$ but the LS estimation of local models (12) is not.

Experience has shown that the segment length should at least be about 15 samples, to ensure low bias and a good estimation efficiency when applying the simulated annealing algorithm. To reduce the algorithm execution time, the segment length should be limited in average to 60 samples; the global minimum is easier to find in a small segment.

B. Merging of Segments

Since the presented process is nonsequential in time and overlaps are allowed between segments, local phases and local amplitudes are merged by means of a weighted sum. The procedure of computing the weights for the merging procedure is explicit in Section C of the Appendix. For this purpose, we use Hamming windows for which the significant weight (see Fig. 2) is placed at the segment center where the error estimation is minimized [24], [25]. Contrary to the Hanning window, the sides of the Hamming window are not equal to zero, which ensures that the estimation on the segment sides is not completely neglected. Since the whole phase estimate results in a weight mean of all the local phases estimated, this ensures respect for the phase continuity constraint assumed in Section I. We proceed similarly for the local amplitudes. Nevertheless, if the difference between the estimated phases in two successive segments is higher than a given threshold[1] Γ_φ, we consider that a phase discontinuity occurs and the algorithm is consequently stopped.

[1]This threshold is an upper bound on the difference between the estimated phases in two successive segments to ensure the phase continuity. Γ_φ is experimentally determined and it is typically equal to $\pi/6$.

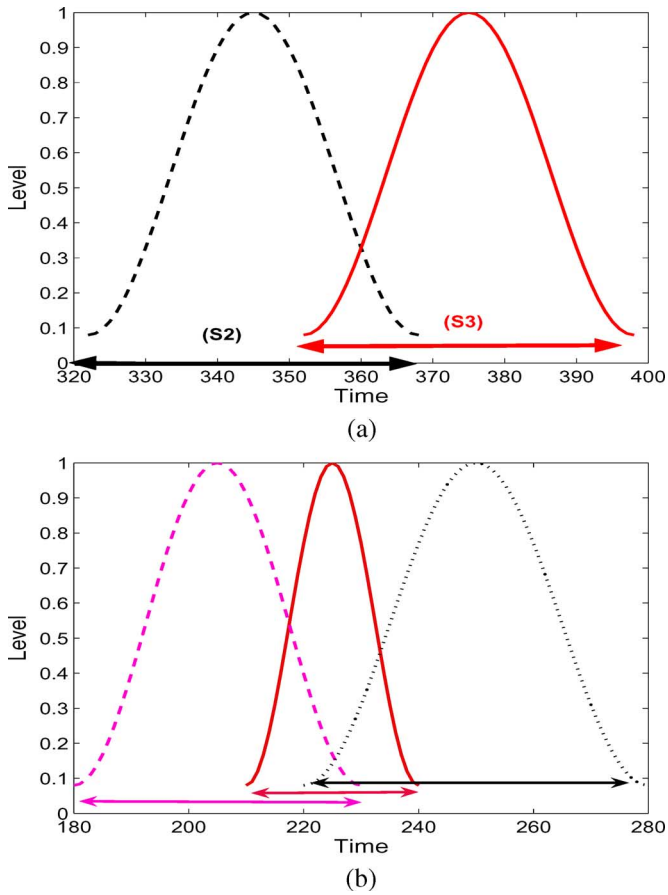


Fig. 2. Merging strategy using Hamming windows for the phase smoothing: Two cases (a) and (b) are possible. (a) Two segments are merged. (b) Three segments are merged.

TABLE II
NONSEQUENTIAL TIME-SEGMENTATION ALGORITHM

1) Calculate $S_y[n, \nu]$ the TFD of $y[n]$ and determine $F_0[n]$ a rough approximation of the IF (15).
2) Locate the energy peak n_0 and ν_0 (16).
3) Use Table I to define the segment to be processed.
4) Estimate the local IA $a[k]$, IF $f[k]$ and the local phase $\varphi[k]$ on the considered segment using a low-order polynomial model and the simulated annealing algorithm (Section II and Section B of the Appendix).
5) If an overlap occurs two cases are possible
   a- if the difference on the local phases of two successive segments is lower than $\Gamma_\varphi = \frac{\pi}{6}$, merge the estimated segments using the merging strategy (Section III-B and Section C of the Appendix).
   b- if not, go to step 8.
6) If the whole observations are processed go to step 8. Otherwise go to the next step.
7) Calculate $S_{y_r}[n, \nu]$ the TFD of the residue $y_r[n]$ (17). Then restart from step 2.
8) The estimation is finished and the signal-estimate output is reconstructed using (2) by using the whole amplitude and phase estimates.

Remark: in all experiments, the spectrogram is used as a non-negative TFD without cross terms .

The steps involved in the whole signal estimation are described in Table II.

C. Discussion

Three particularities of the segmentation strategy contribute considerably to reducing the estimation errors. The first is that this nonsequential strategy starts by estimating the parts of the

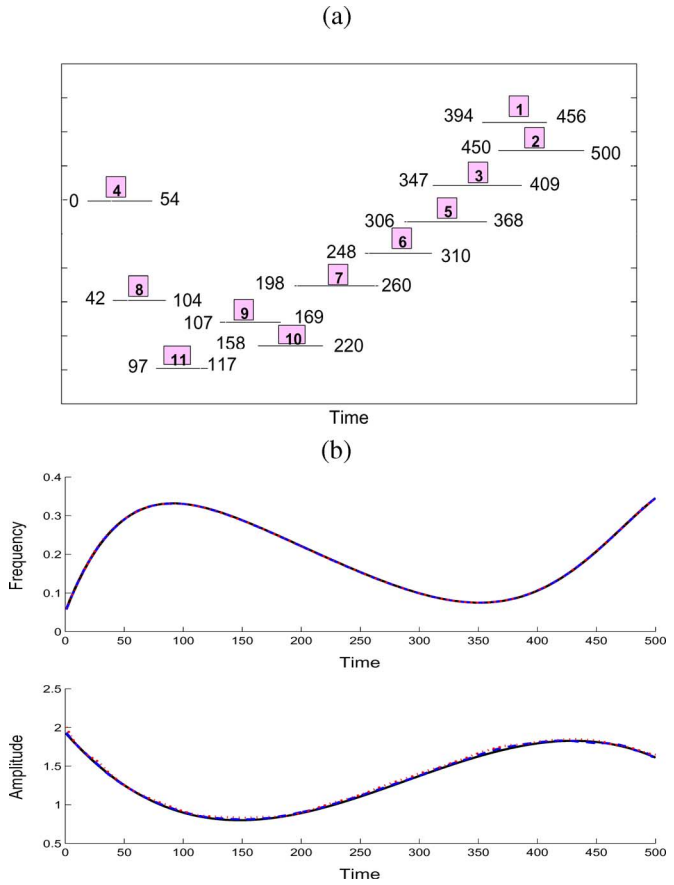


Fig. 3. (a) Nonsequential time segmentation of the signal in Fig. 1. Each segment bears a mention of the starting time, ending time, and processing order (in a box). (b) Estimation of IF (seventh-order polynomial) and IA (cubic polynomial) for the same signal based on the mean of 50 Monte Carlo realizations at a mean SNR equal to 15 dB (- -) and 7 dB ($\cdots$) versus original curves (—).

signal that have the highest energy content. The estimation process on segments where the SNR is locally very low does not affect segments where the SNR is locally high. The second particularity is that segment estimation is done independently of the other segments, thus avoiding error propagation between segments. Making the points of the signal that have the highest energy content coincide with the center of the segments helps to reduce the estimation error [26]. This, of course, constitutes the third particularity. Moreover, this strategy is easy to implement and presents a tradeoff between accuracy and low central processing unit (CPU) time.

Fig. 3(a) illustrates the nonsequential time segmentation of the signal given in Fig. 1. In Fig. 3(b), the estimated IF and IA of this signal are plotted. Since the SNR is time-varying because of the IA changes, we indicate a mean SNR equal to 15 and 7 dB. The IF estimates are very close to the originals at both SNR values. However, the IA estimate at 7 dB deviates slightly from the original IA.

As can be seen, we do not need to estimate degrees and coefficients for the whole AM/FM signal models and local variations of IA and IF are closely tracked. The signal model given by (2) is preserved, since smoothing is applied only to the phase and the amplitude and the signal estimate $\hat{s}[n]$ is reconstructed in step 8) of Table II using (2).

IV. Performance Analysis

In this section, the proposed algorithm is applied to PPS signals and to nonpolynomial AM/FM signals. Comparisons with CRBs and the HAF-based method are also discussed. We use the spectrogram as a nonnegative TFD for the segmentation strategy.

A. CRBs

We give the appropriate CRBs to study statistically the algorithm performance when applied to PPS. We, therefore, consider a signal given by (2), where IA and the phase are given by (4). Three types of CRBs are defined: classical, local, and global CRBs.

1) Classical CRB: In [29], the CRBs denoted by $\mathrm{CRB}_{\mathcal{P}}$ are derived for polynomial amplitudes and frequencies. The $\mathrm{CRB}_{\mathcal{P}}$s are time-varying functions and they make use of the entire signal samples

$$\begin{aligned}\mathrm{CRB}_{\mathcal{P}}\left(A[n]\right) &= \frac{\sigma^2}{2}\boldsymbol{b}^{\dagger}(\boldsymbol{A}^{\dagger}\boldsymbol{A})^{-1}\boldsymbol{b}\\ \mathrm{CRB}_{\mathcal{P}}\left(F[n]\right) &= \frac{\sigma^2}{2}\boldsymbol{h}^{\dagger}(\boldsymbol{\Phi}^{\dagger}\boldsymbol{\Phi})^{-1}\boldsymbol{h}\end{aligned}, \qquad \text{for} \quad 0 \le n \le N-1 \tag{18}$$

with

$$\begin{aligned}\mathbf{A} &= [\boldsymbol{b}_0.e^{j\boldsymbol{\Phi}}, \boldsymbol{b}_1.e^{j\boldsymbol{\Phi}}, \ldots, \boldsymbol{b}_P.e^{j\boldsymbol{\Phi}}]\\ \boldsymbol{\Phi} &= j[\boldsymbol{b}_0.\boldsymbol{s}, \boldsymbol{b}_1.\boldsymbol{s}, \ldots, \boldsymbol{b}_Q.\boldsymbol{s}]\\ \boldsymbol{b} &= [1, n, n^2, \ldots, n^P]^{\mathrm{T}}\\ \boldsymbol{h} &= \frac{1}{2\pi}\left[0, 1, 2n, \ldots, Qn^{(Q-1)}\right]^{\mathrm{T}}\\ \boldsymbol{b}_m &= [0^m, 1^m, 2^m, \ldots, (N-1)^m]^{\mathrm{T}}\\ e^{j\boldsymbol{\Phi}} &= \left[e^{j\Phi[0]}, e^{j\Phi[1]}, \ldots, e^{j\Phi[N-1]}\right]^{\mathrm{T}}\\ \boldsymbol{s} &= [s[0], s[1], \ldots, s[N-1]]^{\mathrm{T}}.\end{aligned} \tag{19}$$

$(.)$ denotes element-by-element multiplication. $(^{\mathrm{T}})$ and $(^{\dagger})$ are the transpose and the transpose conjugate. $\boldsymbol{\Phi}$ and $\boldsymbol{A}$ are matrices of $N\times(Q+1)$ and $N\times(P+1)$ size, respectively. It is important to note that the $\mathrm{CRB}_{\mathcal{P}}$ formulas use the variance value σ^2 of the noise (1) and the order values of polynomial approximations of both the amplitude and the phase (P and Q). Therefore, orders are assumed to be known when we calculate these bounds.

2) Local CRB: In [23], we calculate the appropriate CRBs, denoted by $\mathrm{crb}_l(\boldsymbol{\theta})$, for local-model parameters $\boldsymbol{\theta}$ (8) of short-time signals whose amplitudes and frequencies are modeled as given by (7), and for an orthonormal discrete polynomial base

$$\mathrm{crb}_l(\boldsymbol{\theta}) = \frac{\sigma_l^2}{2}\begin{pmatrix} I_p & 0\\ 0 & \left(\boldsymbol{\Phi}_l^{\dagger}\boldsymbol{\Phi}_l\right)^{-1}\end{pmatrix} \tag{20}$$

where

$$\begin{aligned}\boldsymbol{\Phi}_l &= j[\boldsymbol{\eta}_{-1}.\boldsymbol{s}_l, \boldsymbol{\eta}_0.\boldsymbol{s}_l, \ldots, \boldsymbol{\eta}_q.\boldsymbol{s}_l]\\ \boldsymbol{\eta}_m &= \left[\eta_m\left[\frac{-L}{2}\right], \ldots, \eta_m\left[\frac{L}{2}\right]\right]^{\mathrm{T}}\\ \boldsymbol{s}_l &= \left[s_l\left[\frac{-L}{2}\right], \ldots, s_l\left[\frac{L}{2}\right]\right]^{\mathrm{T}}.\end{aligned} \tag{21}$$

I_p is the identity matrix of $p \times p$ size and $\mathbf{\Phi}_l$ is a matrix of $(L+1) \times (q+1)$ size. $s_l[k]$ is defined in (12) while $\eta_m[k]$ is given by $\eta_{-1}[k] = 1$ and

$$\eta_m[k] = 2\pi \left(\sum_{l=\frac{-L}{2}}^{k} g_m[l] - \sum_{k=\frac{-L}{2}}^{0} g_m[l] \right)$$

for $k \in [-(L/2), (L/2)]$ and $0 \leq m \leq q$. $g_m[k]$ is introduced in (7) and σ_l^2 is the local noise variance on the segment considered. In [23] and [24], we show the MSE of the parameter estimation $(\boldsymbol{\theta})$ closed to the $\text{crb}_l(\boldsymbol{\theta})$ (20) for SNR varying from 0 to 25 dB whereas the HAF-obtained results are far from these CRBs.

The CRBs of the local IA $a[k]$ and IF $f[k]$ are written as

$$\begin{aligned} \text{CRB}_l(a[k]) &= \frac{\sigma_l^2}{2} \sum\nolimits_{m=0}^{p} g_m[k]^2 \\ \text{CRB}_l(f[k]) &= \frac{\sigma_l^2}{2} \boldsymbol{\eta}^\dagger \left(\mathbf{\Phi}_l^\dagger \mathbf{\Phi}_l \right)^{-1} \boldsymbol{\eta} \end{aligned}, \quad \text{for} \quad \frac{-L}{2} \leq k \leq \frac{L}{2} \tag{22}$$

where $\boldsymbol{\eta} = [0, g_0[k], g_1[k], \ldots, g_q[k]]^{\mathrm{T}}$. In this paper, the CRB_ls are used to study the estimation accuracy of local models related to the considered segments.

3) Global CRB: Finally, by assuming that each segment estimation process is independent of the others, we derive new available bounds,[2] that we call CRB_G, which take into account the segmentation process and the smoothing strategy (weighted sum; see Section III-B).

$\text{CRB}_{\mathcal{P}}$s (18) differ basically from CRB_ls (22), and hence from CRB_Gs, through the model definitions. $\text{CRB}_{\mathcal{P}}$s are established for the whole polynomial-phase model (4), in which the entire set of samples and a canonical–polynomial base are used. As known [30], these bounds are the lowest and are very optimistic in highly nonlinear cases whereas CRB_Gs are calculated using CRB_ls (22), and consequently, they are better adapted to the estimation process we developed. In fact, CRB_ls are derived for a local (and short-time) signal model (7), for which the local frequency is modeled instead of the local phase and an orthonormal polynomial base is used. Moreover, the local phase is obtained by a numerical integration of the local frequency and the phase origin is placed at the middle of the segment.

In Section IV-B, CRB_G is shown to be the closest to the estimation variance. Nevertheless, we should be careful when we compare these bounds since they are derived for unbiased estimators, and it is well known that biased estimators can reach lower bounds. Biased estimates can have smaller MSEs than unbiased ones.

B. Simulation Results

In this section, the proposed algorithm is evaluated using numerical examples including a high-order PPS and a nonpolynomial phase signal. Obtained results are compared with the appropriate CRB. A comparison with the results obtained using the HAF-based method is also given.

[2]CRB_G are calculated using the following formula, where x and z are independent estimators and $(\alpha, \beta) \in \mathbb{R}^2$

$$\text{variance}(\alpha x + \beta z) = \alpha^2 \text{variance}(x) + \beta^2 \text{variance}(z).$$

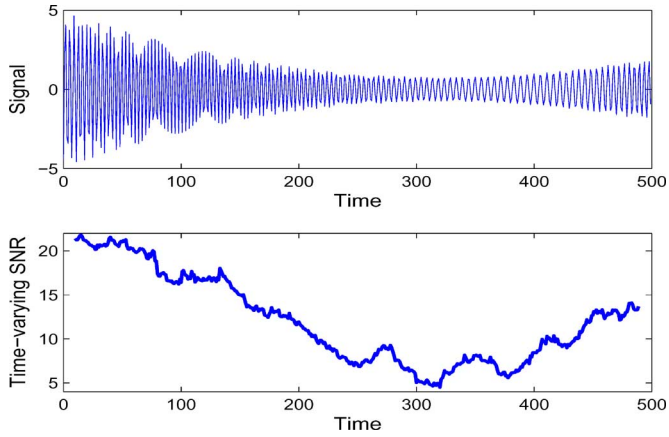


Fig. 4. Noisy signal of (23) and the time-varying SNR (decibels) which is computed by using a sliding window of 20 samples.

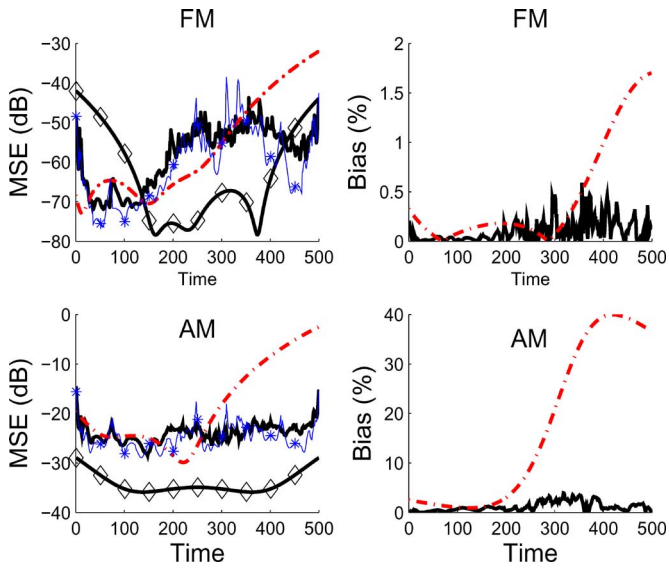


Fig. 5. MSE of the IA and IF estimates of the signal of (23) at a mean SNR = 15 dB: (– · –) HAF-based method, (—) the proposed method, (–◇–) the $\text{CRB}_{\mathcal{P}}$, and (–∗–) the CRB_G.

1) Comparison With the HAF Technique: We consider a signal given by (1) where IF and IA are third- and second-order polynomials written as follows:

$$\begin{aligned} F[n] &= 0.2483 - 7.6474\ 10^{-4}(n-250) \\ &\quad + 1.6796\ 10^{-7}(n-250)^2 + 1.2057\ 10^{-8}(n-250)^3 \\ A[n] &= 0.9747 - 0.0058(n-250) + 3.9447\ 10^{-5}(n-250)^2, \\ &\quad \text{for } 0 \leq n < 500. \end{aligned} \tag{23}$$

The noisy signal and the time-varying SNR are reported in Fig. 4. The phase $\Phi[0]$ is considered to be known only when using the HAF-based method; otherwise, this method is unable to correctly estimate the phase $\Phi[n]$ and the amplitude $A[n]$. The mean SNR is 15 dB and the sample number is 500. We run 100 Monte Carlo noise simulations. The variance of the AM and FM estimation is depicted in Fig. 5 and compared to the CRB_G and $\text{CRB}_{\mathcal{P}}$ which is calculated using (18) with the true order values. We can see that the proposed algorithm performs better than the HAF. Indeed, the HAF-based method presents a

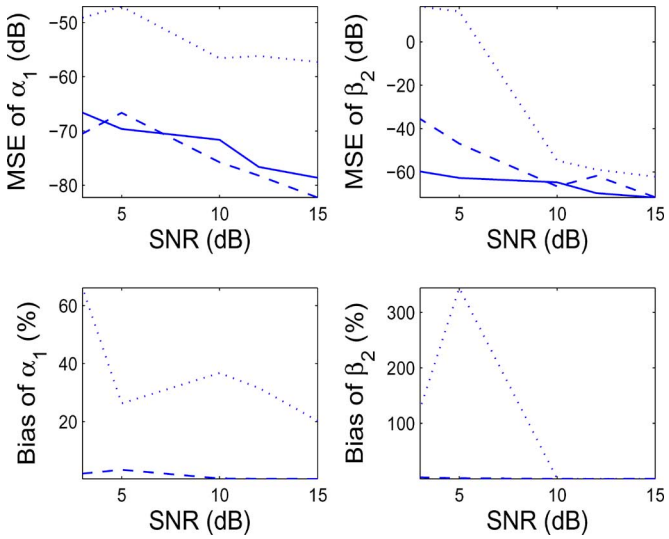


Fig. 6. MSE and bias of the amplitude parameter α_1 and phase parameter β_2 (4) of the signal of (23) versus SNRs: $(\cdots)$ HAF-based method, (- -) the proposed method, and (—) the appropriate CRBs.

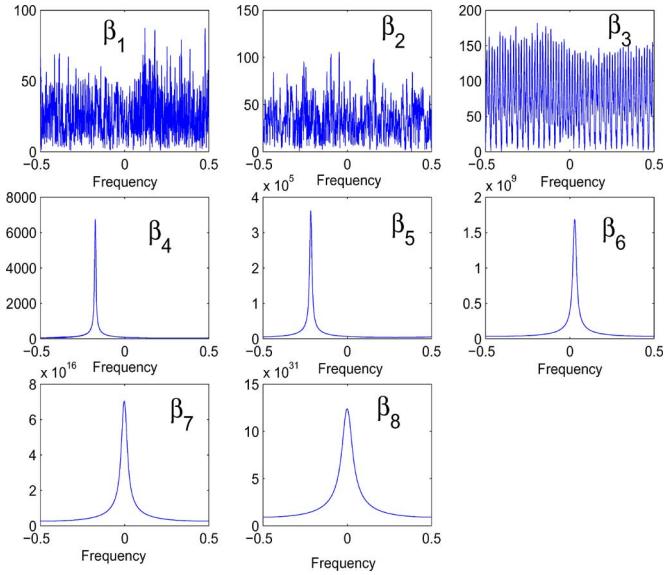


Fig. 7. HAF transform of the signal in Fig. 1 as calculated for the phase coefficients, which are proportional to the peak of the HAF transform [7]. The coefficients are plotted with respect to their order [β_m in (4)]. The SNR is ∞.

large bias and MSE especially on the right side of the window, whereas the SNR is low (see Fig. 4). Since the phase $\Phi[0]$ is given for the HAF-based method, the biases are not high on the left side of the time window.

Moreover, a comparison between the proposed approach and the HAF-based method including CRB curves as a function of the mean SNRs is shown in Fig. 6. We run 100 Monte Carlo noise simulations for each mean SNR and we evaluate the estimates of the amplitude parameter α_1 and the phase one β_2 (4) of the signal given by (23). Fig. 6 shows that both the MSE and bias of these parameter estimates are smaller with the approach proposed than with the HAF method.

Before discussing the deviation from the different CRBs, we apply the HAF-based method to the signal shown in Fig. 1, which was randomly generated. Readers are reminded that the IA is a cubic polynomial and IF is a seventh-order polynomial (the phase order is 8). The sample number is 500 and the sampling frequency is 1 Hz. Since the HAF is an estimation technique that provides the phase coefficient sequentially, the efficiency decreases as far as the order of the polynomial approximation increases. The errors of the highest order coefficient affect the estimate of the lower order coefficients. In Fig. 7, we can see this propagation phenomenon error.

On the contrary, the local maximum-likelihood estimators, which are used in the algorithm proposed, require the joint estimation of all the phase and amplitude coefficients simultaneously. Using a discrete polynomial orthonormal base improves the estimation by decoupling the parameter estimation [23], [24]. Furthermore, error propagation is avoided since each segment is estimated separately. Consequently, when the signal displayed in Fig. 1 is processed by the proposed algorithm, better results are obtained, as shown in Fig. 8(a) and (b). The right column of Fig. 8(a) shows good performance at low SNR. The MSE, obtained in the estimation of FM and AM, and the biases are based on 50 Monte Carlo noise simulations for each mean SNR. A total of 11 segments are treated (see Fig. 3). Naturally, this takes more execution time than the HAF-based method. The CRB_G and the $\mathrm{CRB}_{\mathcal{P}}$, see (18), computed using the true order values 7 and 3 of the polynomial FM and AM, respectively, are also depicted, at mean SNR equal to 15 and 7 dB.

To explain the differences in the performance over time and discuss the deviation from the CRBs, Fig. 9 shows a zoom of the right side of Fig. 8(a) for the time interval $[306, 456]$. Three more curves are superimposed. One curve is the $\mathrm{CRB}_{\mathcal{P}}$ calculated for an FM polynomial order equal to 9 and that of an AM equal to 4. This serves to illustrate that, as shown in Fig. 9, under- or overevaluated orders modify the $\mathrm{CRB}_{\mathcal{P}}$ behavior. We emphasize that it is not necessary to estimate these orders in order to employ the proposed approach, contrary to the techniques presented in Section I-A. The CRB_l from (22), related to each segment processed (three segments $[306, 368]$, $[347, 409]$, and $[394, 456]$), are plotted. For each local model, the local CRB is calculated using both the appropriate low order (equal to two in this case) and the local SNR related to the considered segments (reported in Fig. 9). We note that the SNR is not constant over time due to the AM changes and it can be locally lower than the theoretical SNR (mean SNR). Finally, assuming each segment estimation process is independent of the others, we plot the CRB_G values that take into account the segmentation process and the smoothing strategy.

Based on all the different curves and on Fig. 9, we conclude that the local estimation of IA and IF is biased, the IA biases being larger than the IF biases. Both the IA MSE and the IF MSE obtained are locally close to the CRB_l and consequently close to the CRB_G. The estimation accuracy and robustness are especially high at the sides of the whole time window. Since the $\mathrm{CRB}_{\mathcal{P}}$s are calculated using the all signal samples and established for unbiased estimators, they are very optimistic, especially in the middle of the window.

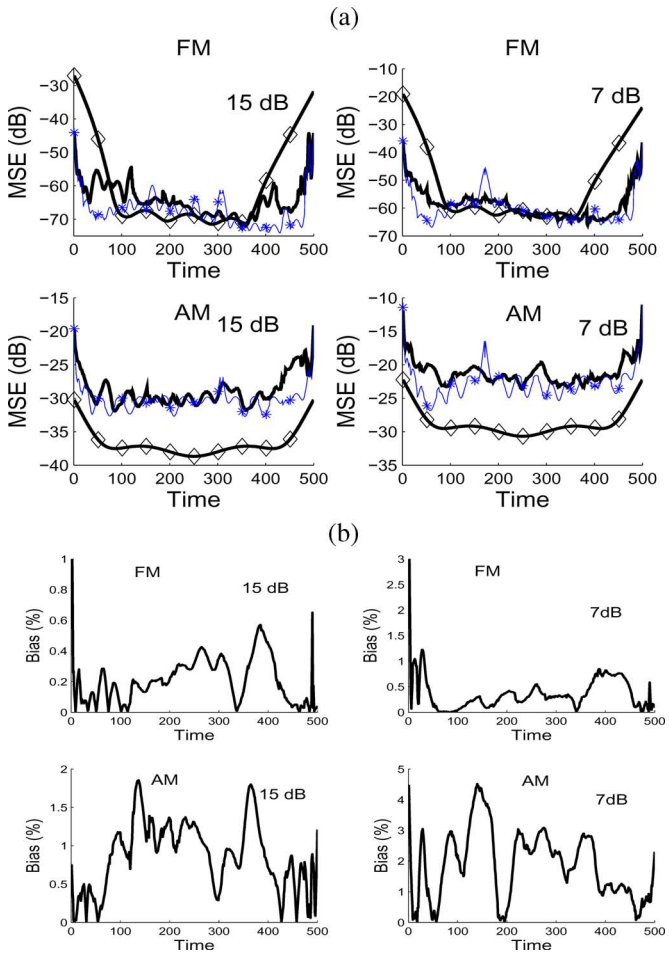


Fig. 8. (a) MSE obtained in the estimation of the frequency and amplitude of the highly nonstationary signal in Fig. 1 using (—) the algorithm proposed, ($-\diamond-$) the CRB$_{\mathcal{P}}$, and ($-*-$) the CRB$_G$, at mean SNR = 15 dB (left column) and at 7 dB (right column). The CRB$_{\mathcal{P}}$ values are calculated at the true orders: the FM is a seventh-order polynomial and the AM is a third polynomial. (b) Biases (—) at mean SNR= 15 dB (left column) and at 7 dB (right column) using the proposed algorithm.

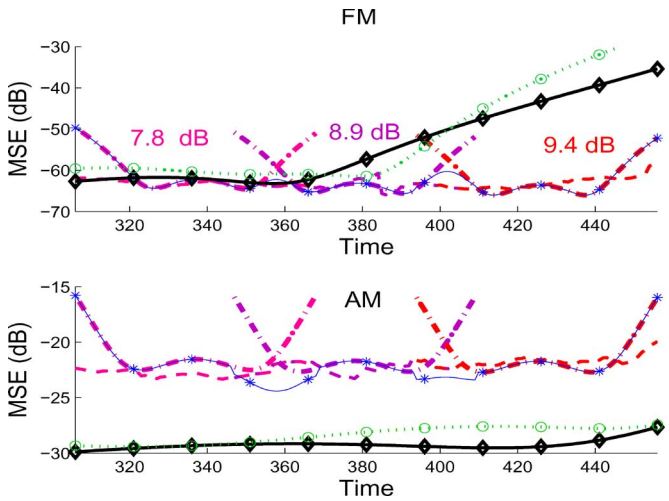


Fig. 9. Zoom in the right column of Fig. 8 (SNR= 7 dB): (- -) MSE and ($-\cdot-$) CRB$_l$ for each segment, ($-\diamond-$) CRB$_{\mathcal{P}}$ calculated for the true orders, ($-\circ-$) CRB$_{\mathcal{P}}$ calculated for FM order = 9 and AM order = 4, and ($-*-$) CRB$_G$ derived after segmentation and smoothing strategies.

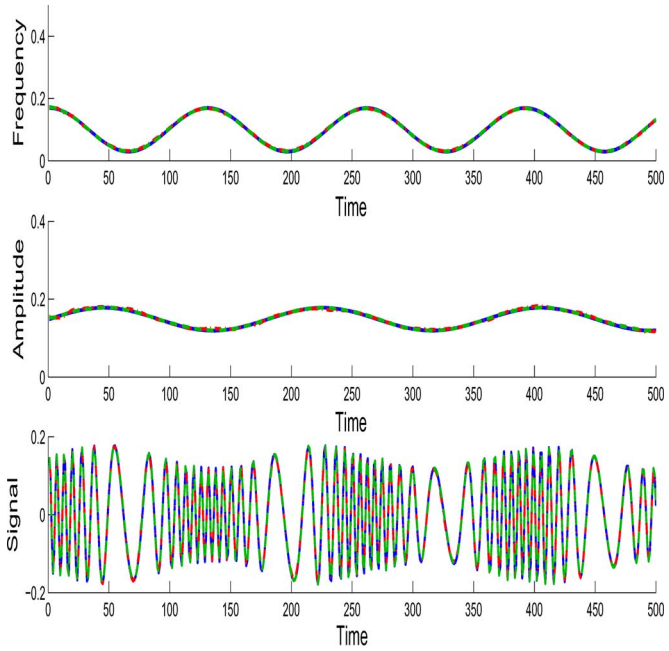


Fig. 10. Original curves of a sinusoidal AM/FM signal (—) and the reconstructed ones: (- -) at 15 dB and ($-\cdot-$) at 7 dB using the proposed algorithm.

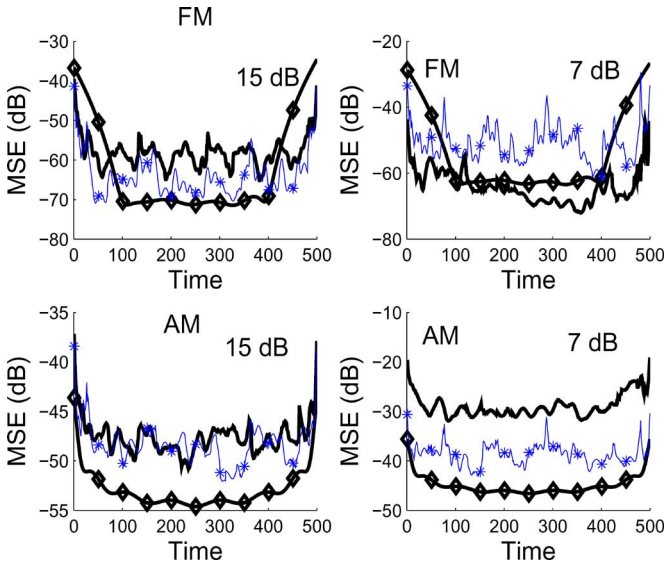


Fig. 11. MSE (- -) of the sinusoidal AM and FM estimates. The CRBs are calculated at a mean SNR = 15 dB (left column) and SNR = 7 dB (right column) for a polynomial approximation of the seventh-order for both AM and FM.

2) Application to Nonpolynomial AM/FM Signals: We consider a sinusoidal AM/FM signal. The signal model is given by (1) where

$$F[n] = 0.1011 + 0.0993\cos(2\pi 0.3840\, n)$$
$$A[n] = 0.1485 + 0.0294\sin(2\pi 0.2786\, n),$$
$$\text{for } 0 \le n \le 500. \tag{24}$$

The phase here is nonpolynomial. Fig. 10 shows the reconstructed curves of AM and FM at mean SNR equal to 15 and 7 dB while Fig. 11 shows the modulation MSE. The CRB$_{\mathcal{P}}$ are calculated for polynomial approximations with an order equal to 7 for AM and FM. A total of 22 segments of an average

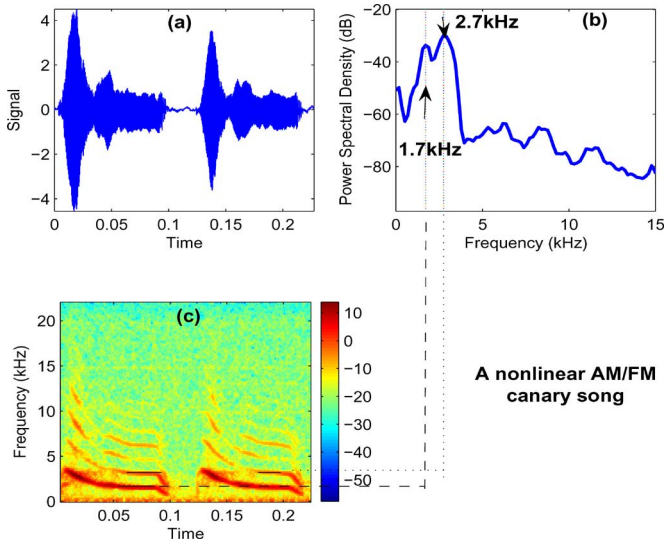


Fig. 12. Canary song: (a) AM/FM signal, (b) power spectral density and (c) spectrogram calculated using a fast Fourier transform of 256 points, a sliding Hanning window of 256-point length, and an overlap of 255.

of 30 samples is processed and merged in order to reconstruct the modulations in their entirety. From Fig. 10, we observe that polynomial models of higher orders are not necessary for estimating the total modulations on the whole time duration. The segmentation process and estimation algorithm proposed are robust in the presence of low SNRs. Other simulations are given in [23] and [24].

V. Real-World Signal

Many acoustic research projects [31] study the sound production in songbirds and try to build mechanical models. Actually, birds generate sound by air-flow-induced[3] vibration of structures in their vocal organ, "the syrinx."[4] The syringeal muscles control gating and frequency in the signal. They can contract extremely fast to modulate the tension and position of the labia, and hence, produce the frequency of the sound emitted. Since songbirds can modulate the amplitude and frequency of their diverse songs over various time scales [31], [32], TF analysis tools applied for the sound help to identify candidates for generators and modulators in the sound production mechanism. The commonly used tool was the spectrogram, but this was limited in the resolution.

In this section, we focus on a canary sound shown in Fig. 12. The frequency sampling of the recorded data is 44 kHz and the SNR is high. The total sample number is 10 000. This is a signal with multiple nonlinear components because of the labia collisions. The IFs decrease exponentially and tend to superimpose on the time intervals [0.09 s, 0.11 s] and [0.20 s, 0.22 s]. The modulation rate is over 4 kHz for each component. Fig. 12(b) depicts the fundamental frequency of the labia oscillations in the syrinx. The presence of the first two harmonically related energy components of 1.7 and 2.7 kHz fundamental corresponds to a tuned filter of the trachea and beak. We propose here to improve

[3]The air-sacs play an important role in vocalization; they provide the pressure difference of bronchial to induce oscillation of the labia in the syrinx.

[4]An organ unique to birds, the syrinx has nonlinear mechanical properties.

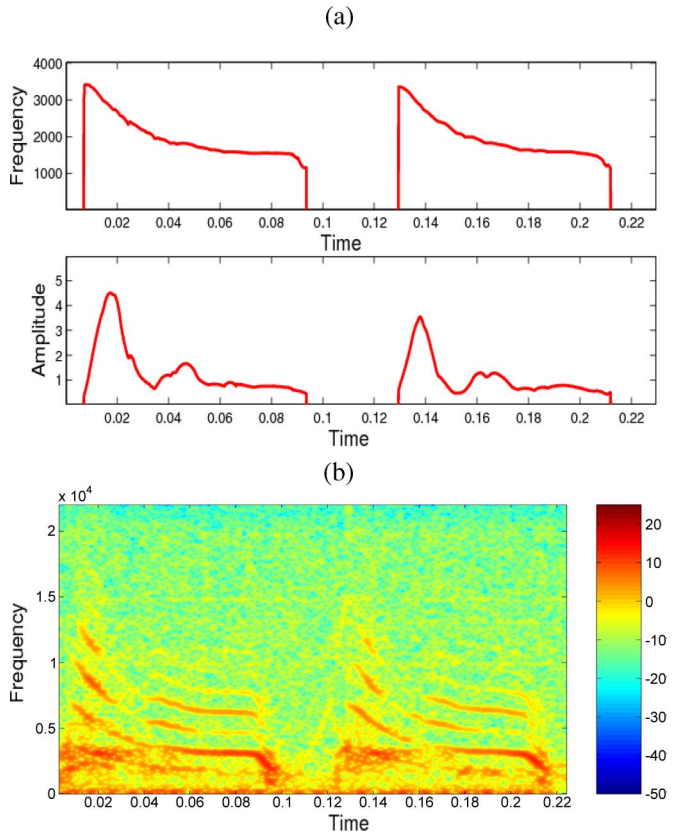


Fig. 13. (a) Estimated FM and AM of the highest energy component of the signal. (b) Spectrogram of the residual signal after removing the highest energy component of the canary song calculated with a fast Fourier transform of 1024 points, a sliding window of 256, and an overlap of 255.

the estimation accuracy by applying the nonsequential segmentation algorithm to only estimate the highest energy component. The estimation of all the components will be investigated in future works. Fig. 13 shows a good estimate of the highest energy component and the residual signal, respectively. Because of the large sample number, 300 segments are processed.

VI. Conclusion

A new method for processing signals with highly nonlinear AM/FM was presented. The proposed approach assumes that the signal nonstationarity could be piecewise modeled by low-order polynomials on short-time windows called segments. To reduce the estimation error, the first segment corresponded to the highest energy part of the signal. Then, a segmentation process was followed in positive or negative time progression in order to estimate the next high-energy part of the signal.

For each segment, low-order polynomials were used for estimating both AM and FM. The polynomial orders were limited to three. The model parameters were then estimated using the maximum-likelihood procedure, which locally preserves the optimality. Since this produces a highly complex equation, a stochastic optimization technique called simulated annealing is applied [23]–[25]. The estimated segments were then merged in order to reconstruct the whole AM/FM signal.

To demonstrate the estimation accuracy of the merging process, the CRBs were given and a comparison to the HAF

was presented. The estimation accuracy of the nonsequential segmentation algorithm was higher than that of the HAF-based method. We show that the proposed method performs well with sinusoidal AM/FM signals and high-order PPS. This approach was applied to a multicomponent real signal to separate the component with the highest energy content from the others. The estimation of all the components will be addressed in future work [33], [34]. Two strategies for estimating the multicomponent signals are possible. One possibility is to iteratively reconstruct the signal component by component, each component being estimated by using the nonsequential algorithm and then removed. The second is to estimate all the components at the same time on local segments having short-time duration and then to apply the merging process.

We can reasonably conclude that the proposed method offers many advantages. For example, no model order needs to be estimated for any of the modulations. On one hand, this avoids an order selection for the entire-phase model, which can be of a high order in the case of strong nonstationarity. On the other hand, the maximum-likelihood estimation of each local model avoids the error propagation phenomenon, which is common with the existing HAF technique. Estimating each segment separately ensures more robustness despite the SNR variations. The proposed method also provides an estimate of the component with the highest energy content when applied to multicomponent signals. The originality of the nonsequential segmentation algorithm is that it is able to fit a wide range of frequency and amplitude waveforms by merging local polynomial models. However, a limit on the validity is imposed by the guarantee to provide low-order polynomial models on segments of reasonable length. Indeed, if the signal modulations become more rapid, we ideally have to change the models in (7) instead of increasing the polynomial order of the local models. Since the algorithm is scalable and easy to implement, other models such as sinusoidal functions and splines will be studied in further work.

APPENDIX

A. Discrete Orthonormal Polynomial Base

Let $\{g_m[k]\}_{m=0,\ldots,\max(p,q)}$ be an orthonormal polynomial base written as

$$g_m[k] = b_{m,0}k^0 + b_{m,1}k^1 + \ldots + b_{m,m-1}k^{m-1} + b_{m,m}k^m$$

for $0 \leq m \leq \max(p,q)$ and $k \in [-L/2, L/2]$. We apply the Gram–Schmidt procedure

$$\langle \boldsymbol{g}_m, \boldsymbol{g}_l \rangle = \sum_{k=\frac{-L}{2}}^{\frac{L}{2}} g_m[k] g_l[k] = \delta_{m,l} \tag{25}$$

where $\boldsymbol{g}_m = [g_m[-L/2], \ldots, g_m[L/2]]^{\mathrm{T}}$ and $\delta_{m,l}$ is the Kronecker symbol. We obtain the following values for an order $m \leq 3$:

$$b_{1,0} = b_{2,1} = b_{3,0} = b_{3,2} = 0$$
$$b_{2,0} = \frac{-\sqrt{5L(L+2)}}{2\sqrt{(L+3)(L+1)(L-1)}}$$
$$b_{2,2} = \frac{6\sqrt{5}}{\sqrt{(L+3)(L+2)(L+1)L(L-1)}}$$
$$b_{1,1} = \frac{2\sqrt{3}}{\sqrt{L(L+1)(L+2)}}$$
$$b_{3,3} = \frac{1}{\sqrt{\sum k^6 - \frac{\left(\sum k^4\right)^2}{\sum k^2}}}$$
$$b_{0,0} = \frac{1}{\sqrt{L+1}}$$
$$b_{3,1} = -\, b_{3,3} \frac{\sum k^4}{\sum k^2}$$

where the symbol $\sum$ denotes the discrete sum from $k = -L/2$ to $L/2$. See [24] for more details.

TABLE III
SIMULATED-ANNEALING-BASED ALGORITHM

1) Initialization $\boldsymbol{\theta} = \boldsymbol{\theta}^{(0)}$,
   Evaluate $\hat{s}_l[k]$ for $\boldsymbol{\theta}$ using (7) and (14).
   Set $\hat{e}_l[k] = y_l[k] - \hat{s}_l[k]$.
2) Repeat until $\hat{e}_l[k]$ is a white process ([33]),
   2.1- Set $\boldsymbol{\sigma}_c^2 = \boldsymbol{\sigma}_0^{2\,(0)}$ and $\mathcal{T} = \mathcal{T}^{(0)}$.
   2.2- Iterations from $t = 1$ to T
      a- Generate $\boldsymbol{\theta}_c = \boldsymbol{\theta} + \Delta\boldsymbol{\theta}$ from a Gaussian distribution $\mathcal{N}(\boldsymbol{\theta}, \boldsymbol{\sigma}_c^2)$.
      b- Draw $\xi \sim \mathcal{U}[0,1]$, if $\xi < \exp(\frac{\ell_{LS}(\boldsymbol{\theta}) - \ell_{LS}(\boldsymbol{\theta}_c)}{\mathcal{T}})$, set $\boldsymbol{\theta} = \boldsymbol{\theta}_c$, otherwise $\boldsymbol{\theta}$ is not modified.
      c- Sample $u \sim \mathcal{B}(\rho)$. If $u = 1$, set $\boldsymbol{\sigma}_c^2 = (1 - \epsilon_\sigma)\,\boldsymbol{\sigma}_c^2$ and $\mathcal{T} = (1 - \epsilon_{\mathcal{T}})\mathcal{T}$.
      d- Evaluate $\hat{s}_l[n]$ for $\boldsymbol{\theta}$ using (7) and (14). Set $\hat{e}_l[n] = y_l[n] - \hat{s}_l[n]$. Go to 2.2.
   2.3- Go to 2.

B. Main Steps of the Simulated Annealing Algorithm

Table III shows the main steps of the simulated annealing algorithm.

$\boldsymbol{\theta}$ is the parameter vector (8), $\boldsymbol{\sigma}_c^2$ is the range search for the parameter values, and $\mathcal{T}$ is the temperature useful for monitoring the algorithm towards the best solution. $\boldsymbol{\theta}^{(0)}$, $\boldsymbol{\sigma}_0^{2(0)}$, and $\mathcal{T}^{(0)}$ are the initialization of $\boldsymbol{\theta}$, $\boldsymbol{\sigma}_c^2$, and $\mathcal{T}$, respectively. Both $\mathcal{T}$ and $\boldsymbol{\sigma}_c^2$ are reduced linearly (step b in Table III) in a random way. $\mathcal{U}$ and $\mathcal{B}$ are uniform and Bernoulli distribution laws. $\ell_{\mathrm{LS}}(\boldsymbol{\theta})$ is the LS function defined in (12). $\hat{s}_l[k]$ is the estimation of $s_l[k]$. Both $s_l[k]$ and $y_l[k]$ are defined in (12). See [35] for more details.

The parameters are initialized as follows:

$$a_i^{(0)} = \left\langle A^{(0)}[n], g_i[n] \right\rangle \tag{26}$$
$$f_i^{(0)} = \left\langle F^{(0)}[n], g_i[n] \right\rangle \tag{27}$$

with

$$A^{(0)}[n] = \left| \mathcal{S}_y\left(n, F^{(0)}[n]\right) \right|. \tag{28}$$

$F^{(0)}[n]$ is given in Section II and $\mathcal{S}_y(n,\nu)$ is defined in (15). $\varphi_0^{(0)}$ is the angle of the Fourier transform of the signal $y[n]$ calculated for a frequency $\nu_\varphi = \arg\max_\nu |\mathcal{S}_y[0,\nu]|$. We have

$$\boldsymbol{\theta}^{(0)} = \left[a_0^{(0)}, a_1^{(0)}, \ldots, a_p^{(0)}, \varphi_0^{(0)}, f_0^{(0)}, f_1^{(0)}, \ldots, f_q^{(0)}\right]^{\mathrm{T}}.$$

C. Weight Computing for Merging Process

Let S_1 and S_2 be two segments and $S_1 \cap S_2$ be their overlap. We note $H_1[n]$ and $H_2[n]$ the Hamming window values and $\hat{\Phi}_1[n]$ and $\hat{\Phi}_2[n]$ the estimated phases where $(._1)$ and $(._2)$ denote values related to the estimated segment S_1 and S_2, respectively. The phase merging is given by

$$\hat{\Phi}[n] = \frac{H_1[n]\hat{\Phi}_1[n] + H_2[n]\hat{\Phi}_2[n]}{\sqrt{H_1[n]^2 + H_2[n]^2}}. \tag{29}$$

By assuming that each segment estimation process is independent of the others, the estimation variance is obtained for $n \in S_1 \cap S_2$ by

$$var\left(\hat{\Phi}[n]\right) = \frac{H_1[n]^2 var\left(\hat{\Phi}_1[n]\right) + H_2[n]^2 var\left(\hat{\Phi}_2[n]\right)}{H_1[n]^2 + H_2[n]^2} \tag{30}$$

and so, we have for $n \in S_1 \cap S_2$

$$\begin{aligned} var\left(\Phi[n]\right) &\geq \frac{H_1[n]^2 \mathrm{CRB}_l\left(\Phi_1[n]\right) + H_2[n]^2 \mathrm{CRB}_l\left(\Phi_2[n]\right)}{H_1[n]^2 + H_2[n]^2} \\ &= \mathrm{CRB}_G\left(\Phi[n]\right). \end{aligned} \tag{31}$$

ACKNOWLEDGMENT

The authors would like to thank Dr. C. Elemans for his help in the explanation of the sound production mechanism of songbirds and his suggestions to ameliorate this paper.

REFERENCES

[1] F. Vincent and O. Besson, "Estimating time-varying DOA and Doppler shift in radar array processing," *Proc. Inst. Electr. Eng.—Radar, Sonar Navigat.*, vol. 147, no. 6, Dec. 2000.

[2] T. F. Quatieri, R. B. Dunn, R. J. McAulay, and T. E. Hanna, "Underwater signal enhancement using a sine-wave representation," in *Proc. IEEE Oceans*, Oct. 1992, pp. 449–454.

[3] F. Leonard, J. Lanteigne, S. Lalonde, and Y. Turcotte, "Vibration behavior of a cracked cantilever beam," *Mech. Syst. Signal Process.*, vol. 15, no. 3, pp. 529–548, 2001.

[4] P. Maragos, J. F. Kaiser, and T. F. Quatieri, "Energy separation in signal modulations with application to speech analysis," *IEEE Trans. Signal Process.*, vol. 41, no. 10, pp. 3024–3051, Oct. 1993.

[5] Z. Guo, L. G. Durand, and H. C. Lee, "Comparison of time-frequency distribution techniques for analysis of simulated Doppler ultrasound signals of the femoral artery," *IEEE Trans. Biomed. Eng.*, vol. 41, no. 4, Apr. 1994.

[6] L. Cohen, P. Loughlin, and D. Vakman, "On an ambiguity in the definition of the amplitude and phase of a signal," *Signal Process.*, vol. 79, pp. 301–307, 1999.

[7] S. Peleg and B. Friedlander, "The discrete polynomial-phase transform," *IEEE Trans. Signal Process.*, vol. 43, no. 8, pp. 1901–1914, Aug. 1995.

[8] G. Zhou, G. B. Giannakis, and A. Swami, "On polynomial phase signals with time-varying amplitudes," *IEEE Trans. Signal Process.*, vol. 44, no. 4, pp. 848–861, Apr. 1996.

[9] A. M. Zoubir and I. Ameer, "Bootstrap analysis of polynomial amplitude and phase signals," in *IEEE TENCON—Speech Image Technol. Comput. Telecommun.*, 1997, pp. 843–846.

[10] C. Theys, M. Vieira, and G. Alengrin, "A reversible jump sampler for polynomial phase signal," in *Proc. ICASSP*, Phoenix, AZ, 1999, pp. 1833–1836.

[11] J. Angeby, "Estimating signal parameters using the nonlinear instantaneous least squares approach," *IEEE Trans. Signal Process.*, vol. 48, no. 10, pp. 2721–2732, Oct. 2000.

[12] S. Saha and S. M. Kay, "Maximum likelihood parameter estimation of superimposed chirps using Monte Carlo importance sampling," *IEEE Trans. Signal Process.*, vol. 50, no. 2, pp. 224–230, Feb. 1995.

[13] H. Cottereau, J. M. Piasco, and M. Davy, "Tow approaches for the estimation of time-varying amplitude multi-chirp signals," in *Proc. ICASSP*, 2003, pp. IV.657–IV.660.

[14] P. O'Shea, "A fast algorithm for estimating the parameters of a quadratic FM signal," *IEEE Trans. Signal Process.*, vol. 52, no. 2, Feb. 2004.

[15] C. Ioana, C. Cornu, and A. Quinquis, "Polynomial phase signal processing via warped higher-order ambiguity function," in *Proc. EUSIPCO*, Vienna, Austria, Sep. 2004, pp. 1159–1162.

[16] A. Abutaleb, "Instantaneous frequency estimation when the amplitude is a stochastic process using stochastic calculus and bootstrapping," *Circuits Syst. Signal Process.*, vol. 24, no. 1, pp. 35–52, 2005.

[17] S. Barbarossa, A. Scaglione, and G. B. G. Nikias, "Product higher order ambiguity function for multicomponent polynomial phase signal modeling," *IEEE Trans. Signal Process.*, vol. 49, no. 3, pp. 691–708, Mar. 1998.

[18] A. Francos and M. Porat, "Analysis and synthesis of multicomponent signals using positive time-frequency distributions," *IEEE Trans. Signal Process.*, vol. 47, no. 2, pp. 493–504, Feb. 1999.

[19] M. Z. Ikram and G. T. Zhou, "Estimation of multicomponent polynomial phase signals of mixed orders," *Signal Process.*, vol. 81, pp. 2293–2308, Nov. 2001.

[20] L. Chung-Chieh and P. M. Djuric, "Estimation of chirp signals by MCMC," in *Proc. ICASSP*, Istanbul, Turkey, 2000, pp. 265–268.

[21] A. O. Boudraa, J. C. Cexus, F. Salzenstein, and L. Guillon, "IF estimation using empirical mode decomposition and nonlinear teager energy operator," in *Proc. ICASSP*, Montreal, QC, Canada, 2004, pp. 45–48.

[22] C. Dubois, M. Davy, and J. Idier, "Tracking of time-frequency components using particle filtering," in *Proc. ICASSP*, Philadelphia, PA, 2005, pp. IV.9–IV.12.

[23] M. Jabloun, M. Vieira, F. Leonard, and N. Martin, "Local orthonormal decomposition for both instantaneous amplitude and frequency of highly nonstationary discrete signals," in *IMA: The Institute of Mathematics and Its Applications*, Cirencester, U.K., Dec. 2004, pp. 107–110.

[24] M. Jabloun, M. Vieira, F. Leonard, and N. Martin, "A AM/FM single component signal reconstruction using a nonsequential time segmentation and polynomial modelling," in *Proc. IEEE Workshop Nonlinear Signal Image Process.*, Sapporo, Japan, May 2005.

[25] M. Vieira, F. Leonard, M. Jabloun, and N. Martin, "Short time single polynomial phase using Legendre functions," in *Proc. EUSIPCO*, Vienna, Austria, Sep. 2004, pp. 793–796.

[26] D. Rife and R. Boorstyn, "Single-tone parameter estimation from discrete-time observation," *IEEE Trans. Inf. Theory*, vol. IT-20, 1974.

[27] M. F. Aburdene, "On the computation of discrete legendre polynomial coefficients," in *Multidimentional Systems and Signal Processing*. Boston, MA: Kluwer, 1993, pp. 181–186.

[28] P. L. Loughlin, J. W. Pitton, and E. Atlas, "Construction of time-frequency distributions," *IEEE Trans. Signal Process.*, vol. 42, no. 10, pp. 2697–2705, Oct. 1994.

[29] B. Friedlander and J. M. Francos, "Estimation of amplitude and phase parameters of multicomponent signals," *IEEE Trans. Signal Process.*, vol. 43, no. 4, pp. 917–926, Apr. 1995.

[30] H. L. V. Trees, *Detection Estimation and Modulation Theory, Part I*. New York: MIT/Wiley, 1968.

[31] C. P. H. Elemans, "How do birds sing? Sound analysis-mechanical modelling-muscular control," Ph.D dissertation, Exp. Zoology Group, Wageningen Univ., Wageningen, The Netherlands.

[32] F. Goller and R. A. Suthers, "Role of syringeal muscles in gating airflow and sound production in singing brown thrashers," *Neurophysiol.*, vol. 75, pp. 867–876, 1996.

[33] M. Jabloun, N. Martin, M. Vieira, and F. Leonard, "Maximum likelihood parameter estimation of short-time multicomponent signals with nonlinear AM/FM modulation," in *Proc. IEEE Workshop Statist. Signal Process.*, Bordeaux, France, Jul. 2005.

[34] M. Jabloun, N. Martin, M. Vieira, and F. Leonard, "Multicomponent signal: Local analysis and estimation," in *Proc. EUSIPCO*, Antalya, Turkey, Sep. 2005.

[35] M. Locatelli, "Convergence and first hitting time of simulated annealing algorithm for continuous global optimization," in *Mathematical Methods of Operations Research*. New York: Springer-Verlag, pp. 171–199.



Meryem Jabloun was born in Tunisia in 1978. She received the Eng. and M.Sc. degrees in digital signal processing and telecommunications from the Ecole Nationale Superieure de l'Electronique et de ses Applications (ENSEA), University of Cergy Pontoise, France, in 2003. Currently, she is working towards the Ph.D. degree at the Laboratoire des Images et des Signaux (LIS), GIPSA lab-Grenoble, Saint Martin d'Heres, France.

Her research interests are the analysis and interpretation of nonstationary signals and models of polynomial phase signals.

Francois Leonard received the M.S. degree in physics from the Ecole polytechnique de Montreal, Montreal, QC, Canada, in 1981.

In 1981, he joined a research team working on wind turbines at the Hydro-Quebec Research Institute, Varennes, QC, Canada, as a Specialist in instrumentation and signal processing. Among other work, he has developed a special modal tool for estimating the low damping modes of wind turbines, the so-called Zmodal. During 1987–1989, he wrote the code for a monitoring system now deployed on every large hydro-turbine at Hydro-Quebec. From 1990 to 1995, he worked on hydro-turbine vibration diagnosis and the krigging of the data base cumulated in monitoring systems. Since then, he has worked on the vibro-acoustical monitoring of electrical equipment, vibro-acoustical crack detection in insulation porcelain, and partial-discharge detection and location in underground power cable networks. He wrote the signal-processing algorithm behind many of the leading-edge commercial products originating from Hydro-Quebec.

Michelle Vieira was born in France, in 1972. She received the M.Sc. and Ph.D. degrees in telecommunication engineering and digital signal processing from the University of Nice Sophia-Antipolis, France, in 1995 and 1999, respectively.

She joined the University of Joseph Fourier where she is currently an Associate Professor. She is also affiliated with the Image and Signal Laboratory (LIS), GIPSA lab-Grenoble, Saint Martin d'Heres, France. Her research interests include the digital signal processing for fault diagnosis and for time-frequency characterization.

Nadine Martin (M'06) received the Eng. and Ph.D. degrees from the Institut National Polytechnique de Grenoble, France, in 1980 and 1984, respectively.

Currently, she is a Senior Researcher at the CNRS-National Center of Scientific Research, and in charge of the research team SD-Surveillance Signal and Diagnostic, a team within the Signal and Image Department, GIPSA lab-Grenoble Image sPeech Signal and Automatic, Grenoble, France. In the signal processing domain, her research interests are the analysis and the interpretation of nonstationary signals. Currently, she is working on signal detection, models of polynomial phase signals, and on time-frequency decision based on random models. In addition of seismic and acoustic signals, vibratory signals are more particularly studied in relation with the physical models. In 2004 and 2005, she was a Scientific Advisor for an automotive industry. She is managing a project on an automatic spectral analyzer (TetrAS). She is the author of more than 90 papers and of a French patent extended to the international community in 2005. She was a co-organizer of a predoctoral course on recent advances in signal processing (Les Houches 1993).

Dr. Martin was a member of the National Council of Universities (CNU) in 2002. She was a co-organizer of the Fourth European Signal Processing Conference (EUSIPCO'88), he Sixth French Symposium on Signal and Image Processing (GRETSI 1997), and a special session on diagnostics and signal processing at IEEE-SDEMPED 1997.